Received: 13 September 2022 | Revised: 4 November 2022 | Accepted: 24 November 2022

DOI: 10.1002/ppap.202200169

RESEARCH ARTICLE

PLASMA PROCESSES AND POLYMERS

Damage to OSG low-*k* films during IPVD deposition of the Ta barrier layer

Alexander O. Serov[1] | **Alexey N. Ryabinkin**[1] | **Alexey S. Vishnevskiy**[2] | **Sergej Naumov**[3] | **Alexander F. Pal**[1] | **Tatyana V. Rakhimova**[1] | **Dmitry S. Seregin**[2] | **Konstantin A. Vorotilov**[2] | **Mikhail R. Baklanov**[4]

[1]Department of microelectronics, Skobeltsyn Institute of Nuclear Physics, Lomonosov Moscow State University (SINP MSU), Moscow, Russian Federation

[2]Research and Educational Center "Technological Center", MIREA — Russian Technological University (RTU MIREA), Moscow, Russian Federation

[3]Leibniz Institute of Surface Engineering (IOM), Leipzig, Germany

[4]European Centre for Knowledge and Technology Transfer (EUROTEX), Brussels, Belgium

Correspondence

Alexey N. Ryabinkin, Department of microelectronics, Skobeltsyn Institute of Nuclear Physics, Lomonosov Moscow State University (SINP MSU), Moscow 119991, Russian Federation.

Email: alex.ryabinkin@gmail.com

Funding information

Russian Science Foundation, Grant/Award Number: 22-29-00763

Abstract

The degradation of a porous organosilicate glass low-*k* dielectric during the ionized physical vapor deposition of tantalum coating is studied. The main contribution to the damage is made by vacuum UV flux (10^{14}–10^{15} s^{-1} cm^{-2}) from the argon inductively coupled plasma of the ionizer, and the effect of the direct current magnetron sputter plasma is small. The damage by vacuum ultraviolet photons with an energy exceeding the band gap of the SiO_2 matrix is associated not only with the removal of carbon-containing groups (terminal CH_3 and bridging CH_2) but also with the breaking of Si–O bonds in the Si–O–Si matrix followed by the formation of hydrophilic Si–OH and Si–H groups. Consequently, the degree of damage can be much higher than would be expected from the depth of CH_3 group depletion.

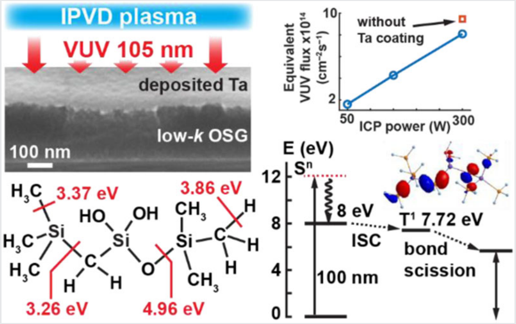

KEYWORDS

absorption, degradation, IPVD, low-k dielectrics, VUV

1 | INTRODUCTION

In modern microelectronics, the need to increase the microchips' performance is hampered by an increase in resistive-capacitive (RC) signal propagation delay in interconnects due to a decrease in the size and distance between the conducting wires.[1,2] To reduce RC delay, low resistivity metals (Cu, Co, Ru, and others) together with low dielectric constant (low-*k*) organosilicate glass (OSG)-based porous dielectrics are used. The OSG materials have structures similar to silicon dioxide, but some of the bridging oxygen atoms in the matrix are replaced by terminal methyl groups, which allows the reduction of the dielectric constant *k* to values lower than that of silicon dioxide. An additional reduction of the *k*-value is achieved by the introduction of porosity.[3,4] However, the methyl-terminated OSG films do not provide the required mechanical strength at $k < 2.5$.[5,6]

because of the reduction of the network connectivity number in the SiO_2-like matrix.[5] The best balance of dielectric constant and mechanical properties has been predicted for OSG materials with organic bridges between silicon atoms and ordered porosity.[7,8] These materials are termed periodic mesoporous organosilica (PMO).[9] However, pure PMO films are not sufficiently hydrophobic, so the addition of methyl-terminated precursors is required.

The copper conductors must be separated from the low-*k* dielectric by a barrier layer (Ta, TaN, etc.) that prevents copper diffusion into the dielectric. The Cu diffusion would otherwise lead to low-*k* degradation.[10] The specific resistivity of the barrier material is usually higher than that of copper, so its thickness should be minimal. An increase in low-*k* porosity not only reduces the *k*-value but also worsens the mechanical strength and makes it difficult to deposit defect-free thin barrier layers since their thickness becomes comparable to the pore size.[11] In addition, porosity increases the damage of low-*k* dielectric during plasma treatment. Therefore, a detailed study of the barrier deposition process is an important issue in modern interconnect technology.

For barrier deposition, ionized physical vapor deposition (IPVD) discharge plasma is usually used, which consists of the plasma of a magnetron sputterer to obtain a stream of sputtered metal atoms, and an inductively coupled plasma (ICP) discharge plasma for their ionization. A high ionization fraction of the sputtered metal atoms is necessary for the deposition of uniform layers on the surface of the grooves (vias and trenches) with a high aspect ratio and for increasing the density of coatings. The effect of plasma on a porous OSG low-*k* dielectric can lead to its damage, which in the case of the barrier deposition has a complicated nature. The degradation of electrical characteristics of integrated structures can be associated with (a) the removal of methyl groups and hydrophilization due to the action of energetic ions and the impact of vacuum ultraviolet (VUV) photons and (b) the penetration of sputtered metal atoms into the porous structure. Removal of methyl groups leads to subsequent moisture adsorption that deteriorates the dielectric properties and reliability of integrated structures.[12] The penetration of sputtered metal atoms can be strongly minimized if the bias potential is not applied.[13,14] Impact of energetic ions has been extensively studied in the case of etch plasmas. Kunnen et al.[15] studied plasma damage in ICP and clearly demonstrated that ion bombardment even reduces plasma damage by oxygen atoms. Similar conclusions were also made by other researchers.[16–18] The common conclusion is that ion bombardment densifies the top surface and formed SiO_2-like “skin” layers that prevent further damage by active radicals.[19] These observations also mean that the depth of damage by ions themselves is limited. In the case of IPVD processes, the deposited barrier layer is an additional factor reducing low-*k* damage by energetic ions. Therefore, if to proceed IPVD barrier process without bias potential, one can expect that the effects of metal atoms penetration and damage by energetic ions might be very small, but the photochemical modification of low-*k* films by VUV photons generated in Ar ICP plasma is much more challenging.

Experience with UV curing of low-*k* materials and damage in the etch and strip plasmas led to the conclusion that the main feature of low-*k* damage is the removal of methyl groups, which is becoming possible when the UV wavelength is less than 200 nm.[20,21] However, VUV photons with energies greater than the band gap can lead not only to the destruction of methyl terminal and bridging methylene bonds but also to the formation of positive charges and vacancies in the SiO_2 matrix and also can break Si–O bonds with the formation of Si–OH and Si–H terminal groups.[22,23] These features were not sufficiently studied in the case of OSG low-*k* materials.

The argon ICP plasma used in the IPVD system emits light with a spectrum exhibiting atomic and ionic emissions with the most intense spectral lines corresponding to the atomic resonance lines, at 104.8 and 106.7 nm, and to the ion lines, at 92.0 and 93.2 nm.[24] All these lines have an energy higher than the bandgap of SiO_2 and OSG materials. The VUV flux of an argon direct current (DC) magnetron discharge plasma was measured by Pal et al.,[25] and the flux was proportional to the discharge current and decreased with pressure. In the experiments of Boffard et al.[26,27] it is shown that the VUV radiation flux in Ar ICP discharge depends nonmonotonically on the gas pressure, reaching maximum values at pressures near 10 mTorr in the case of argon. In numerical simulations, Tian et al.[28] obtained similar results and showed that the ratio of the VUV photon flux to the ion flux increases with increasing pressure. The ion fraction of sputtered atoms depositing the coating depends on the gas pressure, the ICP discharge power, and the power of the magnetron sputtering discharge.[29–32] The presence of sputtered atoms can affect the ICP discharge and VUV radiation, the mutual influence of ICP and DC magnetron plasma on each other and on the transport of sputtered atoms to the substrate as a result of gas heating is also possible.

In the studies mentioned above, the effect of VUV radiation on the low-*k* dielectric from DC magnetron plasma and ICP was studied separately, and in the case of ICP, etching reactors were used, where the ICP coil is located outside the vacuum chamber, while in IPVD setup the coil is usually inside. This, as well as the difficulty of taking into account the possible interplay of the discharges, makes it necessary to measure the damage of low-*k* dielectric by VUV radiation directly in the IPVD process of barrier layer deposition with a high ion fraction of metal atoms.

Taking into account the abovementioned features and challenges, the low-*k* damage was studied during the IPVD deposition of the Ta layer. We have focused on the detailed study of IPVD plasma characteristics using advanced diagnostics and analysis of chemical modification of low-*k* films. In this work, only Ta deposition was analyzed because Ta is usually the first layer directly deposited on the low-*k* surface during Ta-TaN stack formation and the main damage of low-*k* films occurs at this stage. Our results allow confirming that the main damage during the barrier deposition is related to VUV light emitted by Ar plasma and we also analyzed possible bond scission energies in the "damaging" reactions. The bond scission energies were calculated by using quantum chemical calculations as the difference between Free Gibbs energies of molecules in the ground state and products of dissociation.

2 | EXPERIMENT

The IPVD process was carried out in a cylindrical vacuum chamber. The chamber was evacuated to a base pressure of 3.8×10^{-6} Torr using an Edwards 400D turbomolecular pump and an ESVP-600 scroll pump. The working gas pressure was varied in the range of 10–50 mTorr. A mass flow controller MKS GE50A maintained a constant flow rate of 14 sccm argon; the pressure was measured with a capacitance manometer MKS Baratron 626B. Silicon substrates with a deposited low-*k* film were placed on a substrate holder with a rotating mechanism. The substrates were exposed to either ICP or ICP and DC magnetron plasma. Taking into account the features of plasma damage in IPVD processes discussed in Section 1 and elsewhere,[13–18] an additional bias was not applied to the substrate to minimize the energy of the ions bombarding the surface and penetration of metal ions into the dielectric. The threshold energy of Ar ions for breaking the Si–C bond is about 10 eV. Ions with an energy of 10–20 eV damage the uppermost layer of the material with a thickness of about 1 nm.[33] The deposition of a metallic coating should reduce the damage. In this case, the damage is mainly determined by the effect of VUV radiation.[34] The coatings were sputter deposited on the substrates using a DC magnetron sputter source with a water-cooled tantalum target 98 mm in diameter. To increase the ion fraction of sputtered atoms, ICP discharge plasma was used. The discharge was sustained using a single-turn inductor with a diameter of 115 mm constructed using a 6 mm tantalum-coated water-cooled copper tube connected to an RFVII ATN-5 matching device of an RFVII RF-6-XII RF generator with a frequency $f = 13.56$ MHz. The inductor was located 100 mm from the substrate and 85 mm from the sputtering target. One of the ends of the coil was connected to the grounded case of the matching device through an additional RF variable air capacitor according to a scheme similar to that used in the work of Rossnagel and Hopwood.[30] The capacitance of the capacitor was $C \approx 2/(\omega^2 L)$, where L is the inductance of the coil, $\omega = 2\pi f$. The addition of the capacitor to the circuit and its tuning made it possible to reduce the plasma potential (from about 80 to less than 20 V) and the potential difference between the plasma and the coil. This reduced the energy of the ions bombarding the surface of the coil, minimizing its sputtering.

2.1 | Plasma parameter measurements

The plasma parameters in the region of the substrates were measured using an Impedans Langmuir Probe System with RF compensation.[35]

2.2 | Ion fraction of the sputtered atoms measurements

To measure the fraction of ions among the sputtered tantalum atoms depositing the coating (the ion fraction), we used a measuring scheme (Figure 1) based on a quartz crystal microbalance (QCM), similar to those described in Kubart and colleagues.[36,37]

The QCM sensor (1) was mounted in the substrate region instead of the substrate holder. When the sensor was biased to +24 V, sufficient to repel the ions, the deposition rate only by neutral atoms R_A was recorded. When the sensor was grounded, the deposition rate of atoms and ions R_{AI} was measured. The ion fraction α was determined as follows: $\alpha = (R_{AI} - R_A)/R_{AI}$. To protect the QCM measuring crystal from plasma electrons, a magnetic field of permanent rectangular magnets (3) on the magnetic conductor (2) in front of the crystal was used. In contrast to Kubart and colleagues,[36,37] in our case, the use of electric filters for DC isolation of the QCM sensor turned out to be not very effective due to the presence of the RF discharge plasma in the immediate vicinity of the sensor. Instead,

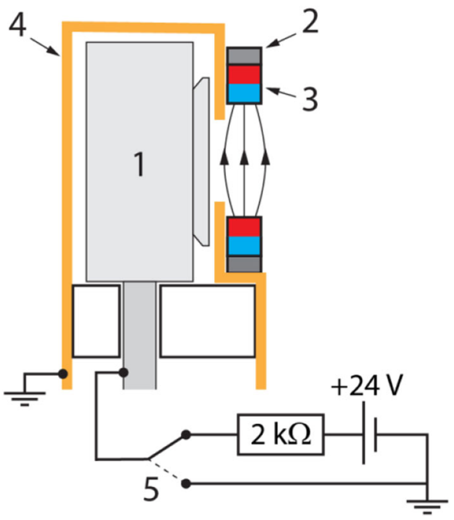

FIGURE 1 Measuring scheme of the ion fraction of sputtered atoms: 1 is the quartz crystal microbalance sensor, 2 is the magnetic conductor, 3 are the permanent magnets, 4 is the grounded casing, and 5 is the switch.

we completely isolated the QCM sensor, its controller, and the computer that controls it from the ground by connecting them to an uninterruptible power supply disconnected from the mains. A +24 V bias was applied to the QCM from batteries through a 2 kΩ resistor. The body of the QCM sensor, with the exception of the hole with the measuring crystal, was covered with a grounded metal casing (4). This made it possible to minimize the interference of the RF discharge on the QCM sensor.

2.3 | Low-*k* films

We used a 100 mm diameter one-side-polished (100) p-Si:B wafer with a resistivity of ~12 Ω • cm. The films with methylene bridges were prepared by using commercially available precursors and special procedures designed for this purpose.[38] The acid-catalyzed (HCl, 37%; Sigma-Aldrich) condensation of alkylalkoxysiloxane–methyltrimethoxysilane (MTMS > 98%; Fluka) and alkylene-alkoxysilane–1,2-bis(triethoxysilyl)methane (BTESM, 97%; abcr) in tetrahydrofuran (THF, anhydrous; 99.9%, Sigma-Aldrich) in the presence of deionized water was used as a film-forming solution. MTMS contains terminal methyl groups while BTESM contains methylene bridges between the silicon atoms. BTESM (45 mol.%) was mixed with MTMS (55 mol.%). Appropriate amounts of MTMS, BTESM, THF, water, and acid were added to a flask fitted with a magnetic stirrer. The water content per methoxy/ethoxy group in the solution was 0.6. The (MTMS + BTESM):HCl mole ratio was 1:0.0002. The final equivalent Si content in the solutions was 6.5 wt%. Porogen Brij® L4 ($C_{12}H_{25}(OCH_2CH_2)_4OH$) from Sigma-Aldrich, with a molar mass of 362 g mol^{-1}, was used as a template in the evaporation-induced self-assembly (EISA) process[39] to control the films' porosity. The porogen concentration was kept equal to 25 wt% to the sum of MTMS and BTESM. The films spin-on deposited on Si wafers were soft-baked on a hot plate at $T_a = 200°C$, 30 min, and the final curing (hard bake) was carried out at $T_a = 430°C$, 30 min in N_2. Mechanical properties were determined by the methods described in Mogilnikov and colleagues.[40,41] The thickness of the film was 250 nm. The film had an open porosity of 40%, a pore radius of 1.7 nm, and Young's modulus of 2.8 GPa as measured by ellipsometric porosimetry.[3,40] The capacitance–voltage curves were collected in the frequency range of 1–100 kHz by using an Agilent 4284 A LCR (inductance [L], capacitance and resistance) meter and MDC 802–150 mercury probe station with a contact diameter of 810 μm from materials development corporation (MDC). The results of these measurements allowed us to evaluate the *k* value of the pristine film on the conductive silicon wafer. For this purpose, a satellite sample with a low-*k* film deposited on a highly doped silicon wafer was used. The measured permittivity was $k = 2.4$.

2.4 | Chemical composition and structure of low-*k* films

The chemical composition and structure of low-*k* films before and after plasma treatment were studied with Fourier transform infrared spectroscopy (FTIR) on a Thermo Electron Corporation Nicolet 6700 spectrometer. IR absorption spectra were recorded in the transmission mode with a resolution of 4 cm^{-1} in an extended range of wavenumbers $\nu = 400–7400$ cm^{-1} and averaged over 64 scans. The background spectra of the silicon substrate were recorded after the mechanical removal of the low-*k* film from the piece located on the initial wafer near the samples under study. The IR spectra of low-*k* films were obtained by dividing the single-beam spectrum of the sample (I_s) by the single-beam background spectrum (I_b), followed by the negative logarithm of the result: $-\log_{10}(I_s/I_b)$. For each sample, 4–10 spectra were recorded at different points and averaged to reduce the noise arising from changes in the background, mainly due to atmospheric contaminations. The baseline was corrected using a 14–16 order polynomial function in combination with a sigmoidal function. The baseline for the Si–CH_3 peak was obtained after spectrum deconvolution in the region of the Si–O–Si band as the sum of all decomposition peaks but Si–CH_3.

For each sample, the relative content of Si–OH, O-H, Si–H, and Si–CH_3 bonds was determined as the ratio of the corresponding peak areas in the IR spectrum to the area of the Si–O–Si asymmetric stretching band.

2.5 | Estimation of VUV radiation flux

To estimate the equivalent VUV flux on the substrate, we used a model developed by Rakhimova and colleagues,[42,43] in which damage to OSG low-*k* dielectric by VUV radiation is described by two fundamental parameters: the radiation photoabsorption cross section σ_{PA} and the effective quantum yield φ of Si–CH_3 photodissociation, which takes into account the probability of reattachment of CH_3 back to dangling bonds –Si. According to the NIST database,[44] tantalum has no emission below 200 nm, while argon emission in this region consists mainly of resonance lines of atoms (104.8 and 106.7 nm) and ions (92 and 93.2 nm). We can use $\sigma_{PA} = 4 \times 10^{-17}\ \mathrm{cm}^2$ and $\varphi = 0.4$ for the similar low-*k* dielectric[43] but without methylene bridges to approximately estimate the equivalent VUV flux density.

3 | RESULTS AND DISCUSSION

3.1 | Characteristics of plasma in the IPVD of Ta layers

The ICP parameters were measured in the substrate region. The dependences of the electron concentration and temperature on the RF discharge power and gas pressure are shown in Figure 2. The corresponding plasma potential varied in the range from 16.3 to 18.7 V.

The observed increase in the electron temperature with a power increase above 100 W is due to the effect of gas heating at high power levels, when the gas temperature rises faster at high power levels, as a result of which the concentration of gas atoms decreases faster than the electron concentration increases.[45]

The dependences of the ion fraction of sputtered Ta atoms forming a coating on the substrate on ICP power and on gas pressure for DC magnetron discharge current $I_M = 0.3$ A are shown in Figure 3.

The rapid increase in the Ta ion fraction when the gas pressure increases from 10 to 35 mTorr is due to an increase in the electron concentration (Figure 2b) and a decrease in the mean free path of Ta atoms, which increases the residence time in the plasma. The ion fraction reaches saturation at 35 mTorr, and the further increase in pressure does not lead to a significant increase in ion fraction. The dependence of ion fraction on ICP power is not so strong. Similar dependencies were observed by Rossnagel.[29] The ion fraction increases with ICP power, reaching a maximum in the region of 100 W; a further increase in power leads to a slight decrease in the ion fraction. The decrease is apparently due to gas heating, as indicated by the ICP power dependence of deposition rate (Figure 4) and electron temperature (Figure 2a), which reaches a minimum at the same power value at which the ion fraction reaches the maximum. The energy of ions bombarding the surface of the ICP coil varies depending on the ICP power in the range of 40–60 eV. The corresponding Ta sputtering yield is quite small,[46] so the contribution of the coil sputtering can be neglected.

The deposition of Ta coatings on the substrates of low-*k* dielectric was carried out at a pressure of 35 mTorr, at which the maximum fraction of ions in the stream of sputtered atoms is reached (Figure 3b). The coatings were deposited at ICP power of 50, 150, and 300 W at the same magnetron sputter current $I_M = 0.3$ A. Since the deposition rate depends on the discharge power (Figure 4a), the deposition time for each case was chosen so as to obtain coatings of the same thickness of 5 nm. Deposition conditions are shown in Table 1.

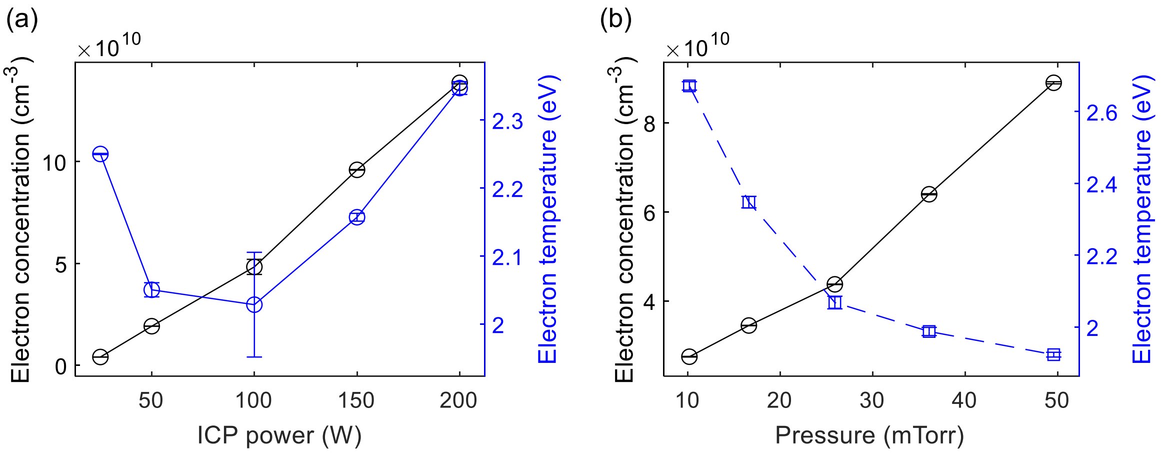

FIGURE 2 Dependencies of the electron concentration and temperature on the inductively coupled plasma discharge power at a pressure of 35.4 mTorr (a) and on the pressure at a power of 100 W (b).

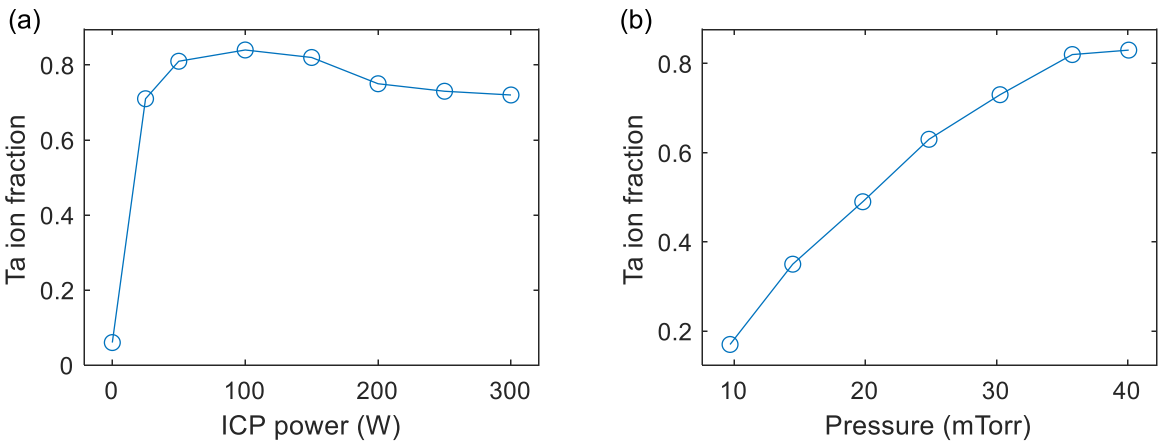

FIGURE 3 Dependence of the ion fraction of sputtered atoms on the inductively coupled plasma (ICP) discharge power at 35 mTorr (a) and on gas pressure at ICP discharge power of 175 W (b). $I_M = 0.3$ A.

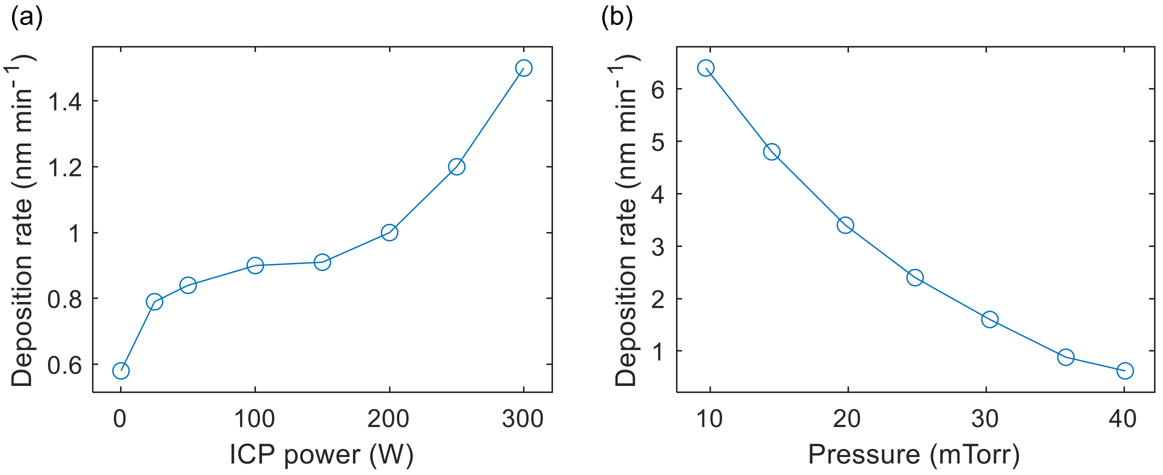

FIGURE 4 Dependence of the deposition rate on the inductively coupled plasma (ICP) discharge power at 35 mTorr (a) and on gas pressure at ICP discharge power of 175 W (b). $I_M = 0.3$ A.

TABLE 1 Process conditions for deposition of Ta coatings on the substrates of low-*k* materials: ICP power (P_{ICP}), DC magnetron discharge current and voltage range (I_M and U_M), gas pressure (p), the ICP coil self-bias (U_{SB}), deposition time (t).

Sample #	P_{ICP} (W)	I_M (A)	U_M (V)	p (mTorr)	U_{SB} (V)	t (s)
0 (pristine)	—	—	—	—	—	—
1 (50/0.3)	50	0.30	229–220	35.97	−31.2	357
2 (150/0.3)	150	0.30	213–218	35.54	−33.3	329
3 (300/0.3)	300	0.31	206–209	35.21	−45.3	200
4 (300/0)	300	—	—	35.42	−44.8	200

Abbreviations: DC, direct current; ICP, inductively coupled plasma.

3.2 | Chemical composition (FTIR data)

IR absorption spectra of deposited and cured samples (pristine, sample #0) and after ICP Ar plasma exposure at different conditions are shown in Figure 5. The most important components of the OSG low-*k* matrix are represented by Si–O–Si asymmetric stretching band (1000–1200 cm^{-1}) and Si–CH$_3$ symmetric bending peak located near 1275 cm^{-1}. The presented spectra were analyzed after baseline correction. Figure 5b shows the deconvolution of the Si–O–Si band region into Suboxide, Network, and Cage (~1027, 1063, and 1145 cm^{-1}, respectively);[47] Si–O–C (~1202 cm^{-1})[47] and Si–CH$_3$ (~1275 cm^{-1})[48] peaks. Vibrations of the Si–C bond near

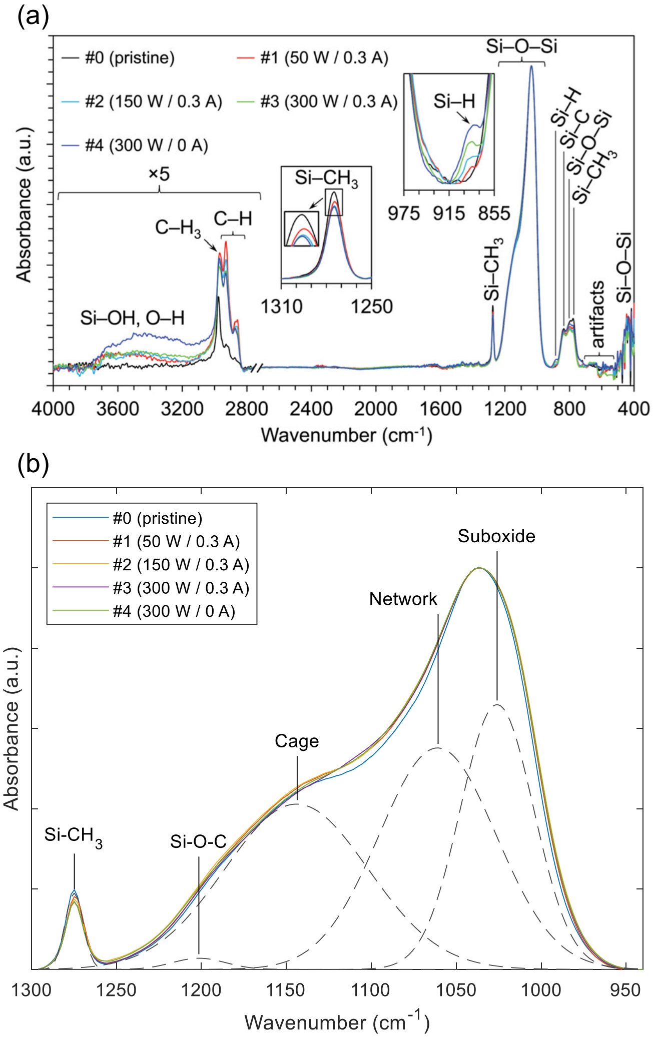

FIGURE 5 (a) Fourier transform infrared spectra of samples. The absorption intensity was normalized to the highest Si–O–Si peak. (b) Infrared absorption spectra of low-*k* films after various exposures to the ionized physical vapor deposition process plasmas in the Si–O–Si asymmetric stretching band region and an example of approximation for sample #0 by the Gaussian peaks (dashed lines) of Si–O–Si Suboxide, Network, and Cage (~1026, 1061, and 1144 cm^{-1}),[47] Si–O–C (~1202 cm^{-1})[47] and Si–CH_3 (~1275 cm^{-1}).[48] This graph clearly shows that no shift in the Si–O–Si absorption peak occurs after exposure to vacuum ultraviolet.

1275 cm^{-1}, in addition to the terminal methyl groups Si–CH_3, can be also due to the bridging carbon group Si–CH_2–Si. In our case, however, no splitting of the peak is observed, which indicates that the contribution of Si–CH_2–Si is small. Figure 5b shows that there is no shift of Si–O–Si peak to larger wavenumbers, which normally happens after strong plasma damage. This correlates with a small change in Si–CH_3 peak intensity and suggests that the degree of carbon depletion is small. The amount of CH_3 groups is normally considered the most direct indicator of plasma damage. Exposure of methyl-terminated OSG films to nonoptimized etch and strip plasmas significantly reduces the intensity of this peak and makes the film hydrophilic.[49] Usually, the removal of CH_3 groups qualitatively increases the intensity of the peak corresponding to Si–H groups,[50] which are hydrophilic and together with adsorbed moisture have a negative impact on low-*k* properties and reliability.

Figure 6 shows that the change in the Si–CH_3 concentration in our case is relatively small and does not exceed 20% of the initial amount. However, the change in the concentrations of the Si–H and Si–OH groups, which are more important for the electrical characteristics of low-*k* dielectrics, is much stronger. The concentration of both Si–H and Si–OH increases almost 10 times. It could also be mentioned the increase in the concentration of carbon-containing groups (2800–3000 cm^{-1}). All these changes are becoming especially pronounced in sample #4, which was exposed to 300 W of ICP power. These results suggest that the samples are damaged by the IPVD plasmas and the degree of damage strongly depends on ICP power.

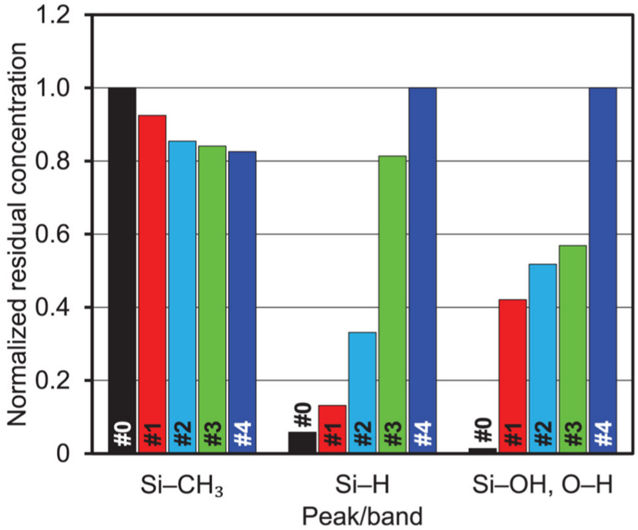

FIGURE 6 Dependence of the residual concentration of Si–CH_3 (1275 cm^{-1}), Si–H (860–900 cm^{-1}), and Si–OH, O–H (3000–3700 cm^{-1}) bonds on the power of the inductively coupled plasma discharge during the deposition of a 5 nm coating.

However, the nature of the damage is different from the one in the case of etch and strip plasmas.

3.3 | VUV radiation flux on the substrate

Figure 7 shows the obtained dependences of the equivalent VUV flux on the ICP power. The presented results were generated from FTIR-measured loss of methyl groups using the approach developed in Rakhimova and colleagues[42,43] and described above in Section 2.5.

In the case of dielectrics with methylene bridges, an additional mechanism of Si–CH_3 group formation due to the breaking of methylene bridges, described in the next section, is possible, which can be roughly taken into account as follows. Assuming that the breaking of methylene bridges is accompanied by the formation of Si–CH_3 bonds with probability k, we can write the equations similar to Equation (5) from Rakhimova et al.[42]:

$$\frac{d[\mathrm{CH_3}](t,z)}{dt} = -I(z)\times\sigma_{PA}\times[\varphi_1\times[\mathrm{CH_3}](t,z) - k\times\varphi_2\times[\mathrm{Si{-}CH_2{-}Si}](t,z)], \quad (1)$$

$$\frac{d[\mathrm{Si{-}CH_2{-}Si}](t,z)}{dt} = -I(z)\times\sigma_{PA}\times[\varphi_2\times[\mathrm{Si{-}CH_2{-}Si}](t,z)], \quad (2)$$

where φ_1 and φ_2 are the effective quantum yields of Si–CH_3 and Si–CH_2–Si photodissociation correspondingly,

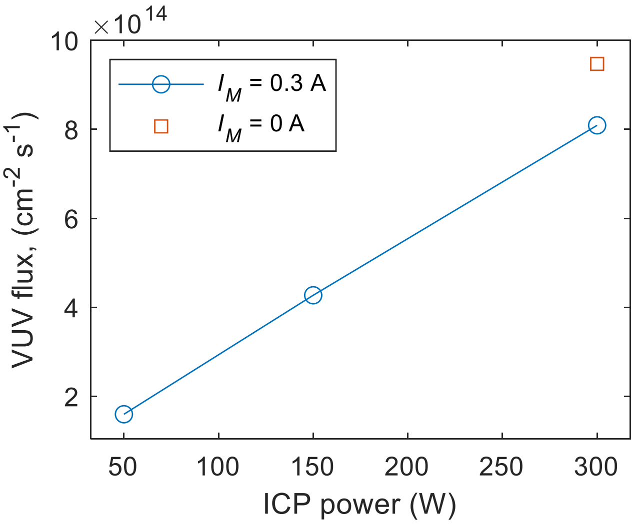

FIGURE 7 Dependence of the equivalent vacuum ultraviolet flux on the inductively coupled plasma discharge power

$I(z) = I_0\exp(-\sigma_{PA}\times[\mathrm{Si}]\times z)$, I_0 is the intensity of the incident VUV radiation. Concentrations are given in square brackets. In the pristine sample $[\mathrm{Si{-}CH_3}]/[\mathrm{Si}] = 0.38$ and $[\mathrm{Si{-}CH_2{-}Si}]/[\mathrm{Si}] = 0.31$, hence $[\mathrm{Si{-}CH_2{-}Si}] = 0.8[\mathrm{Si{-}CH_3}]$. The depletion rates of [Si–CH_2–Si] and [Si–CH_3] under the exposure of 147 nm radiation were obtained in Zotovich et al.[51] for the same low-k dielectrics as in our case. During the first 60 s [Si–CH_2–Si] and [Si–CH_3] decreased linearly, and the decrease rate of [Si–CH_2–Si] was 1.2 times higher than one of [Si–CH_3]. Assuming that $\varphi_1 = \varphi_2$, and $[\mathrm{Si{-}CH_2{-}Si}](t,z) = 0.8[\mathrm{Si{-}CH_3}](t,z)$ we obtain $k = 0.4$, that is, about 40% of the destroyed methylene bridges go to the formation of Si–CH_3 bonds. Taking this into account gives only a 1.5 times higher VUV flux than in Figure 7 and can be ignored.

3.4 | Mechanisms of modification

VUV-induced damage is a complex process that simultaneously changes different characteristics of OSG low-k material. It can change the chemical composition and degrade the electrical characteristics, increasing leakage current and dielectric constant, and reducing the electrical reliability of integrated structures.[49,52,53] The major understanding of VUV damage has been through the intensive experimental study of UV-assisted thermal curing using VUV light with $\lambda = 172$ nm (Xe_2 × excimer emission) and broadband light >200 nm (different kinds of Hg lamps). It has been demonstrated that the degradation of low-k films is mainly associated with the destruction of the hydrophobic Si–CH_3 groups. It was experimentally shown that the chemical composition and electrical characteristics OSG low-k films deteriorate significantly when using VUV light with $\lambda = 172$ nm while do not change when using broadband light with a $\lambda > 200$ nm.[21] Quantum-chemical calculations on model substances similar to OSG fragments show that there is a threshold wavelength of ~190 nm (6.5 eV) for the excitation of the $SiCH_3$ molecule to the first excited singlet state. At this energy, the scission of the $Si–CH_3$ bond may occur, gaining an energy benefit of around 50 kcal mol^{-1}. These findings reveal the presumption that only photons with $E \geq 6.5$ eV ($\lambda < 200$ nm) can generate Si-centered radicals that subsequently attract protons from neighboring methyl groups. Therefore, the concentration of Si–H bonds that can play a role in hydrophilic adsorption centers for water molecules should be directly related to the amount of the removed CH_3 groups. The water adsorption increases the dielectric constant and leakage current of low-k films. Marsik et al.[50] studied the damage of low-k film by VUV light 172 nm (7.2 eV) and demonstrated a quantitative correlation between the reduction of $Si–CH_3$ concentration and the increase of Si–H groups concentration. For this reason, it has been accepted that the concentration of $Si–CH_3$ groups in the low-k matrix is the direct indicator of plasma damage. Generally, it is valid for the most of studies related to plasmas used for low-k patterning and UV curing of low-k dielectrics although the damage during plasma etching might be an even more complicated process due to the synergetic action of VUV light and chemically active radicals[54,55] as well as more complex emission spectra of VUV light. However, in most cases, the loss of CH_3 groups is still an effective indicator of plasma damage.

In our study, in contrast to the results published in Marsik et al.,[50] we found that the formation of Si–H groups significantly exceeds the loss of methyl groups. Therefore, the modification mechanism is different than in most cases associated with UV curing and plasma etching. To understand this, it is necessary to take into account the peculiarities of SiO_2 modification when the photon energy exceeds the band gap (8.9 eV for SiO_2).[56,57] The review article[21] (and references there) discusses and summarizes the analysis of the impact of VUV photons on SiO_2 and methyl-terminated OSG low-k dielectrics, including those with energies exceeding the band gap of SiO_2. In the case of SiO_2, trap cross-sectional spectroscopy[58] and electron spin resonance (ESR) was used to analyze the effects of exposure of SiO_2 to VUV (10 eV) photons.[59,60] Using $Al–SiO_2–Si$ structure, the formation of protons through the interaction of photo-generated holes with atomic hydrogen released from the top gate electrode[61] was suggested. The VUV-induced damage of SiO_2 can be represented as the proton-assisted electrochemical reduction of the oxide resulting in the formation of surface silanol and trivalent Si center[10]:

$$O_3 \equiv Si - \begin{pmatrix} H \\ \vdots \\ O \end{pmatrix}^{+} - Si \equiv O_3 + e^- \rightarrow O_3 \equiv Si - OH + \bullet Si \equiv O_3. \tag{3}$$

It was also shown that the trivalent Si can easily be passivated and de-passivated at room temperature by exposure to atomic hydrogen[62,63]:

$$O_3 \equiv Si \bullet + H \rightarrow O_3 \equiv SiH, \tag{4}$$

or

$$O_3 \equiv SiH + H \rightarrow O_3 \equiv Si \bullet + H_2. \tag{5}$$

Furthermore, ESR data reveal that rupture of the second Si–O bond of the same silicon atom in the $O_3 \equiv Si\bullet$ center occurs with a significantly higher probability than the initial break of the Si–O–Si bridge. This would mean that the damage will cluster eventually leading to the formation of well-defined oxygen-deficient regions. Exposure of methyl-terminated OSG low-k materials to 10 eV photons shows similar mechanisms of defects generation but new features appear from the presence of hydrocarbons. UV/VUV irradiation of low-k dielectrics also affects their properties through several physical mechanisms.[64] First, photogeneration[64] or photo-injection[65] of mobile charge carriers results in their trapping leading to the formation of built-in charges. High hydrogen content makes the formation of protons even more probable than in the case of thermal a-SiO_2 layers explaining the dominance of positive protonic charges after irradiation or electrical stress of low-k insulating layers.[66]

Interesting behavior is demonstrated by low-k films when they were capped by the thin metal layer. A 15-nm thick layer of aluminum was deposited in a vacuum on the unheated sample surface. The presence of such Al dramatically increases the concentration of atomic hydrogen released by VUV photons[59] by (probably) preventing its out-diffusion. In Al-covered CVD1 low-k films[67] after 106 s exposure to 10 eV photons, various new effects are observed,[21,56] but their discussion is beyond the scope of this paper. These observations probably suggest the importance of hydrogen atoms in OSG matrix degradation.

In our work, we also have a different type of low-k material that contains not only methyl terminal groups but also methylene bridges between the Si atoms. Therefore, taking into account the different structures of low-*k* film and UV light wavelength with energy exceeding the bandgap of silica matrix, several additional reactions are becoming possible. These are

1. Detachment of CH_3 groups (similar to $\lambda > 147$ nm)
2. Breaking of Si–O bonds in silica matrix forming surface silanol Si–OH, Si–H, and oxygen deficient centers
3. Detachment of hydrogen atoms from hydrocarbon fragments
4. Destruction of Si–CH_2–Si bridges with the formation of Si–CH_2• and Si• centers

The reduction of CH_3 concentration increases with ICP power. This is expectable because the intensity of VUV radiation increases with ICP power, and therefore, it can be interpreted as a rise in VUV damage. For the same reason, the concentration of Si–H group and adsorbed water increased (Figure 6). One issue is related to the fact that the increase in the concentration of Si–H is significantly higher than the decrease in the concentration of Si–CH_3 groups. Two possible mechanisms can be considered. The simplest explanation is that the low-*k* matrix is modified similarly to pure SiO_2 due to the interaction of the Si–O–Si bond with atomic hydrogen. In this case, the concentrations of the Si–H and Si–OH groups increase much faster than the concentration of the Si–CH_3 groups decreases. The second possible mechanism is related to the relatively low VUV resistance of methylene bridges.[68] Destruction of methylene bridge forms Si–CH_2• and Si• radical groups after saturation by atomic hydrogen increases the concentration of both Si–CH_3 and Si–H groups. Therefore, the evolution of CH_3 concentration has a complicated mechanism (reduction due to the scission of Si–CH_3 bond and increase during the breaking of Si–CH_2–Si bridges) and in this case, it cannot be considered a good indicator of plasma damage in the case of VUV photons with energy exceeding the bandgap of SiO_2. The Si–H groups are hydrophilic, and their concentration is an indicator of the degree of low-*k* damage. The contribution of the DC magnetron discharge plasma turns out to be small and lies within the measurement error.

Another interesting question is related to plasma damage in the presence of sputtered Ta and without it. A good example is the comparison of samples #3 (300W-ICP/0.3A) and #4 (300W-ICP). If you look at the change of Si–H and Si–OH concentrations, then the higher damage of sample #4 is strongly pronounced. We have already mentioned that the presence of a metal layer can significantly change the features of the damage, but in our case, when we analyze the change in the chemical composition, the explanation based on the protective properties of the Ta barrier is the simplest. de Marneffe et al.[69] studied damage of OSG low-*k* films by 147 nm UV light generated in ICP plasma and found that the presence of a thin top mask significantly reduces VUV damage. It was shown that the presence of thin masks based on metal oxides is more efficient than a dielectric mask. The degree of damage was 5–7 times lower than on blanked low-*k* samples.

3.4.1 | Quantum chemical calculations of the bond dissociation energies

The presented experimental results show that the chemical reactions accompanying the photochemical modification of OSG low-k material in argon plasma during IPCVD are significantly different from those previously observed during UV curing. The presence of carbon bridges between silicon atoms in the low-k matrix even increases the number of possible reactions. The experimental analysis of all these reactions constitutes a special physicochemical problem. However, valuable information related to the Gibbs Free energies of the bond's scission can be obtained using quantum chemical calculations.

Quantum chemical calculations were performed in the gas phase on the model molecule including the chemical bonds present in our films (shown in Figure 8) using DFT PBE0-D3/6-31G** level of the theory[70–73] as implemented in the Jaguar 9.6 program.[74] The excited states were calculated using the time dependent (TD) DFT method[75] at the same PBE0-D3/6-31G** level of theory. The dissociation energy (E_{diss}) of a possible bond breaking in the model molecule was calculated as the difference between the Free Gibbs energies of the molecule in the ground state and the products of dissociation. The results of calculations are shown in Figure 8. After excitation into the electronically excited S^n state and relaxation into the first excited singlet state S1, followed by intersystem crossing (ISC), the triplet state will be built. This triplet state has sufficient energy to undergo different bond scissions.

One can see that the chemical bonds present in our OSG film can be separated into two different groups from the point of view of dissociation energy. As expected, the weakest chemical bonds ($E < 85$ kcal/mol) are represented by Si–C bonds from Si–CH_2–Si bridge (R1 and R4), and the bonds between the silicon atom and the terminal methyl group (R2 and R3). The detachment of hydrogen atoms also occurs relatively easily (R5 and R6). One can see that the difference between R1 and R4,

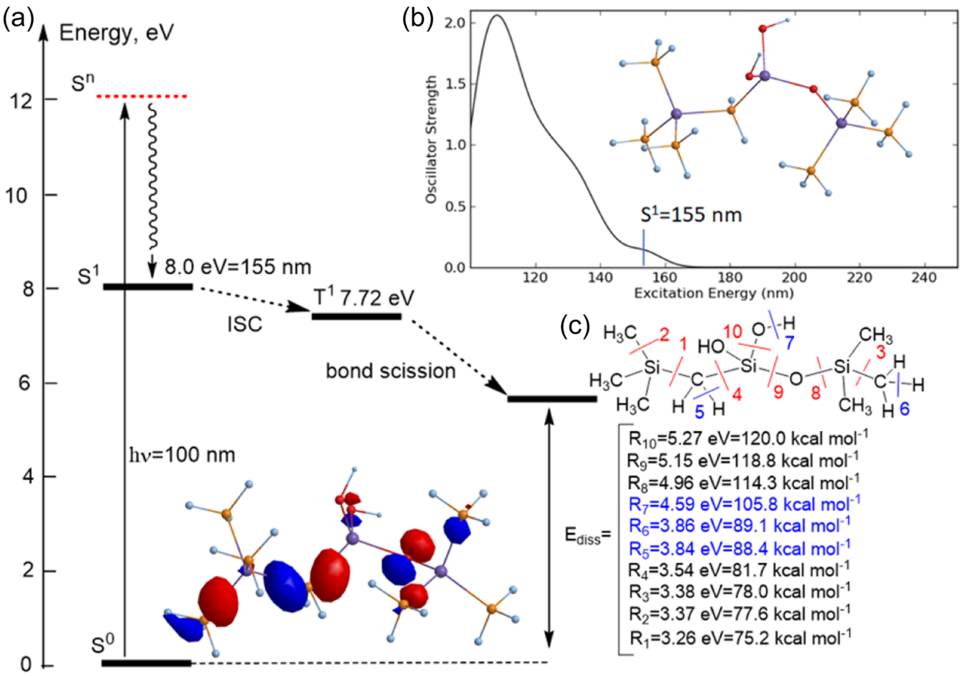

FIGURE 8 (a) Jablonsky diagram, electron distribution from highest occupied molecular orbital (HOMO) in the molecule in the singlet ground state; (b) calculated vacuum ultraviolet (VUV)- spectra after excitation with VUV light with $\lambda = 100$ nm; (c) schema of the possible bond scission in the model molecule with corresponding dissociation energy calculated as the difference between Free Gibbs energies of molecule in ground state and products of dissociation.

R2 and R3, and R5 and R6 reflects the influence of neighboring groups and is easily understandable. For example, R1 < R4 and R8 < R9, since the central Si atom is bonded to the hydroxyl (R10) and, therefore, has a positive charge that enhances the bonding energy with the neighboring CH_2 group and the oxygen atom (R9). The bonds R1 < R2 and R3, indicate that the Si bond with the bridging methylene group is the weakest in this molecule.

The second group of chemical bonds has dissociation energy >100 kcal/mol and includes Si–O bonds (R8 and R9) and also the detachment of the hydroxyl group (R10) and detachment of the H atom from hydroxyl.

It should be noted that in previous work related to understanding low-*k* damage during the UV-assisted thermal curing (UV light with $\lambda = 172–200$ nm), it was found that UV damage is associated only with the removal of CH_3 terminal groups at $\lambda < 190$ nm.[20] In the present work, VUV light with wavelengths of 104.8 and 106.7 nm destroys not only Si–CH_3 bonds but also Si–O and Si–CH_2–Si bonds in the film matrix. However, the degree of damage is limited to the surface part of the films due to the high absorption and low penetration depth of VUV radiation.[22,43,76] The stronger change in the concentration of Si–H groups compared to the depletion of CH_3 is related to the breaking of Si–O bonds with the formation of Si–H and Si–OH groups, as well as the destruction of methyl bridges with the formation of Si–CH_3 and Si–H bonds.

Finally, a feature of our experiments is the demonstration that the damage mechanisms of our films by VUV radiation ~105 nm involve certain reactions observed in pure SiO_2 due to the photon energy exceeding the binding energy between Si and oxygen. However, the presence of different types of carbon compounds complicates the behavior of these films even more and increases the number of possible reactions leading to low-*k* degradation. The most important feature is that the relatively easy release of hydrogen atoms (Figure 8) significantly increases the concentration of hydrophilic SiH groups according to Equations (3–5). Therefore, the resulting depth of the damage can be significantly higher than the depth of depletion of the CH_3 groups. This fact must be taken into account when analyzing the electrical characteristics of integrated interconnect structures.

4 | CONCLUSION

The effect of VUV light from argon ICP plasma radiation on low-*k* dielectric during the deposition of Ta barrier coatings in the IPVD process was studied. The dependences of the plasma parameters, the ion fraction of the sputtered atoms forming the coating, and the deposition rate on the ICP discharge power and working gas pressure are obtained. The damage of low-*k* dielectric as a function of the ICP power of the ionizer was obtained. The equivalent VUV radiation flux was calculated. The flux density is about 10^{14}–10^{15} photons s^{-1} cm^{-2} and is a linear function of the discharge ICP power. Under the experimental conditions, the contribution of the DC magnetron discharge plasma radiation turned out to be negligibly small.

It is concluded that low-*k* damage under the action of VUV radiation with an energy exceeding the band gap of the SiO_2-like matrix is associated not only with the removal of carbon-containing groups (terminal CH_3 and bridging CH_2 groups) but also with the breaking of Si–O bonds in Si–O–Si matrix followed by the formation of hydrophilic Si–OH and Si–H groups. It is shown that low-*k* modification by such VUV photons generates hydrophilic centers SiH exceeding the methyl groups depletion. This observation is important since the concentration of Si–CH_3 cannot always be used as a quantitative criterion for plasma damage. The energy characteristics of the chemical reactions that determine the plasma damage to OSG low-*k* material are calculated and compared. The hydrophilic centers adsorb water molecules during the storage in air. The concentration of these centers is the most important sign of plasma damage in the IPVD system used since the adsorbed water increases the dielectric constant and leakage current of low-*k* films.[5]

ACKNOWLEDGMENTS

The study was supported by the Russian Science Foundation grant No. 22-29-00763.

CONFLICT OF INTEREST

The authors declare no financial or commercial conflict of interest.

DATA AVAILABILITY STATEMENT

Research data are not shared.

ORCID

Alexey N. Ryabinkin http://orcid.org/0000-0002-9277-9431
Alexey S. Vishnevskiy https://orcid.org/0000-0002-4024-5411
Dmitry S. Seregin https://orcid.org/0000-0002-6371-9632
Konstantin A. Vorotilov https://orcid.org/0000-0003-4675-2067
Mikhail R. Baklanov https://orcid.org/0000-0002-9677-1293

REFERENCES

[1] R. Brain, *2016IEEEInt. Electron Devices Meet. (IEDM)*, IEEE, San Francisco, California, USA, **2016** 9.3.1.
[2] Z. Tokei, *2016 IEEE Int. Intercon. Technol. Conf./Adv. Metal. Conf.* IEEE, San Jose, California, USA, **2016**, 1.
[3] M. R. Baklanov, K. P. Mogilnikov, *Microelectron. Eng.* **2002**, *64*, 335.
[4] A. P. Palov, M. R. Baklanov, S. Wei, *J. Vac. Sci. Technol. B* **2019**, *37*, 010601.
[5] D. J. Michalak, J. M. Blackwell, J. M. Torres, A. Sengupta, L. E. Kreno, J. S. Clarke, D. Pantuso, *J. Mater. Res.* **2015**, *30*, 3363.
[6] W. Volksen, R. D. Miller, G. Dubois, *Chem. Rev.* **2010**, *110*, 56.
[7] H. Li, J. M. Knaup, E. Kaxiras, J. J. Vlassak, *Acta Mater.* **2011**, *59*, 44.
[8] Ö. Dag, C. Yoshina-Ishii, T. Asefa, M. J. MacLachlan, H. Grondey, N. Coombs, G. A. Ozin, *Adv. Funct. Mater.* **2001**, *11*, 213.
[9] P. Van Der Voort, D. Esquivel, E. De Canck, F. Goethals, I. Van Driessche, F. J. Romero-Salguero, *Chem. Soc. Rev.* **2013**, *42*, 3913.
[10] M. Hecker, R. Hübner, in *Advanced Interconnects for ULSI Technology* M. R. Baklanov, P. S. Ho, E. Zschech (Eds: M. R. Baklanov, P. S. Ho, E. Zschech), John Wiley & Sons, **2012**, Ch. 6.
[11] X. Wang, L.-T. Liu, P. He, X.-P. Qu, J. Zhang, S. Wei, Y. A. Mankelevich, M. R. Baklanov, *J. Phys. D: Appl. Phys.* **2017**, *50*, 405306.
[12] C. Wu, Y. Li, M. R. Baklanov, K. Croes, *ECS J. Solid State Sci. Technol.* **2015**, *4*, N3065.
[13] L. Zhao, H. Volders, M. Baklanov, Z. Tőkei, M. Pantouvaki, C. J. Wilson, E. Van Besien, G. P. Beyer, C. Claeys, *Microelectron. Eng.* **2011**, *88*, 3030.
[14] M. Krishtab, J.-F. de Marneffe, S. Armini, J. Meersschaut, H. Bender, C. Wilson, S. De Gendt, *Appl. Surf. Sci.* **2019**, *485*, 170.
[15] E. Kunnen, M. R. Baklanov, A. Franquet, D. Shamiryan, T. V. Rakhimova, A. M. Urbanowicz, H. Struyf, W. Boullart, *J. Vac. Sci. Technol. B: Nanotechnol. Microelectron.* **2010**, *28*, 450.
[16] M. A. Goldman, D. B. Graves, G. A. Antonelli, S. P. Behera, J. A. Kelber, *J. Appl. Phys.* **2009**, *106*, 013311.
[17] K. Takeda, Y. Miyawaki, S. Takashima, M. Fukasawa, K. Oshima, K. Nagahata, T. Tatsumi, M. Hori, *J. Appl. Phys.* **2011**, *109*, 033303.
[18] S.-W. Hwang, G.-R. Lee, J.-H. Min, S. H. Moon, *Surf. Coat. Technol.* **2003**, *174–175*, 835.
[19] E. T. Ryan, J. Martin, K. Junker, J. J. Lee, T. Guenther, J. Wetzel, S. Lin, D. W. Gidley, J.ianing Sun, *Proc. IEEE 2002 Int. Intercon. Technol. Conf. (Cat. No.02EX519).* IEEE, **2002**, 27.
[20] L. Prager, P. Marsik, L. Wennrich, M. R. Baklanov, S. Naumov, L. Pistol, D. Schneider, J. W. Gerlach, P. Verdonck, M. R. Buchmeiser, *Microelectron. Eng.* **2008**, *85*, 2094.
[21] M. R. Baklanov, V. Jousseaume, T. V. Rakhimova, D. V. Lopaev, Y. A. Mankelevich, V. V. Afanas'ev, J. L. Shohet, S. W. King, E. T. Ryan, *Applied Phys. Rev.* **2019**, *6*, 011301.
[22] F. A. Choudhury, H. M. Nguyen, S. W. King, C. H. Lee, Y. H. Lin, H. S. Fung, C. C. Chen, W. Li, D. Benjamin,

J. M. Blatz, Y. Nishi, J. L. Shohet, *Appl. Phys. Lett.* **2018**, *112*, 082902.
[23] K. Yokogawa, Y. Yajima, T. Mizutani, S. Nishimatsu, K. Suzuki, *Jpn. J. Appl. Phys.* **1990**, *29*, 2265.
[24] S. Espinho, E. Felizardo, J. Henriques, E. Tatarova, *J. Appl. Phys.* **2017**, *121*, 153303.
[25] A. F. Pal, A. N. Ryabinkin, A. O. Serov, D. V. Lopaev, Y. A. Mankelevich, A. T. Rakhimov, T. V. Rakhimova, M. R. Baklanov, *J. Phys. D: Appl. Phys.* **2020**, *53*, 295202.
[26] J. B. Boffard, C. C. Lin, C. Culver, S. Wang, A. E. Wendt, S. Radovanov, H. Persing, *J. Vac. Sci. Technol., A: Vac. Surf. Films* **2014**, *32*, 021304.
[27] J. B. Boffard, C. C. Lin, S. Wang, A. E. Wendt, C. Culver, S. Radovanov, H. Persing, *J. Vac. Sci. Technol., A: Vac. Surf. Films* **2015**, *33*, 021306.
[28] P. Tian, M. J. Kushner, *Plasma Sources Sci. Technol.* **2015**, *24*, 034017.
[29] S. M. Rossnagel, *J. Vac. Sci. Technol. B: Microelectron. Nanometer Struct.* **1994**, *12*, 449.
[30] S. M. Rossnagel, J. Hopwood, *Appl. Phys. Lett.* **1993**, *63*, 3285.
[31] C. A. Nichols, *J. Vac. Sci. Technol. B: Microelectron. Nanometer Struct.* **1996**, *14*, 3270.
[32] J. Hopwood, *Phys. Plasmas* **1998**, *5*, 1624.
[33] A. P. Palov, O. V. Proshina, T. V. Rakhimova, A. T. Rakhimov, E. N. Voronina, *Plasma Processes Polym.* **2021**, *18*, 2100007.
[34] J. Lee, H. Kazi, S. Gaddam, J. A. Kelber, D. B. Graves, *J. Vac. Sci. Technol. A* **2013**, *31*, 041303.
[35] Impedans Ltd. https://www.impedans.com
[36] T. Kubart, M. Čada, D. Lundin, Z. Hubička, *Surf. Coat. Technol.* **2014**, *238*, 152.
[37] K. Bernátová, M. Fekete, P. Klein, J. Hnilica, P. Vašina, *Plasma Sources Sci. Technol.* **2020**, *29*, 055010.
[38] D. S. Seregin, S. Naumov, W.-Y. Chang, Y.-H. Wu, Y. Wang, N. M. Kotova, A. S. Vishnevskiy, S. Wei, J. Zhang, K. A. Vorotilov, M. Redzheb, J. Leu, M. R. Baklanov, *Thin Solid Films* **2019**, *685*, 329.
[39] Y. Lu, R. Ganguli, C. A. Drewien, M. T. Anderson, C. J. Brinker, W. Gong, Y. Guo, H. Soyez, B. Dunn, M. H. Huang, J. I. Zink, *Nature* **1997**, *389*, 364.
[40] K. P. Mogilnikov, M. R. Baklanov, *Electrochem. Solid-State Lett.* **2002**, *5*, F29.
[41] I. S. Ovchinnikov, A. S. Vishnevskiy, D. S. Seregin, A. A. Rezvanov, D. Schneider, A. S. Sigov, K. A. Vorotilov, M. R. Baklanov, *Langmuir* **2020**, *36*, 9377.
[42] T. V. Rakhimova, A. T. Rakhimov, Y. A. Mankelevich, D. V. Lopaev, A. S. Kovalev, A. N. Vasil'eva, O. V. Proshina, O. V. Braginsky, S. M. Zyryanov, K. Kurchikov, N. N. Novikova, M. R. Baklanov, *Appl. Phys. Lett.* **2013**, *102*, 111902.
[43] T. V. Rakhimova, A. T. Rakhimov, Y. A. Mankelevich, D. V. Lopaev, A. S. Kovalev, A. N. Vasil'eva, S. M. Zyryanov, K. Kurchikov, O. V. Proshina, D. G. Voloshin, N. N. Novikova, M. B. Krishtab, M. R. Baklanov, *J. Phys. D: Appl. Phys.* **2014**, *47*, 025102.
[44] A. Kramida, Y. Ralchenko, J. Reader, NIST ASD Team. *NIST Atomic Spectra Database (Version 5.9)*, National Institute of Standards and Technology, Gaithersburg, MD **2021**.
[45] H.-C. Lee, B. H. Seo, D.-C. Kwon, J. H. Kim, D. J. Seong, S. J. Oh, C.-W. Chung, K. H. You, C. Shin, *Appl. Phys. Lett.* **2017**, *110*, 014106.
[46] W. Eckstein, in *Sputtering by Particle Bombardment: Experiments and Computer Calculations from Threshold to MeV Energies* (Eds: R. Behrisch, W. Eckstein), Springer, Berlin, Heidelberg **2007**.
[47] A. Grill, D. A. Neumayer, *J. Appl. Phys.* **2003**, *94*, 6697.
[48] A. A. Rezvanov, A. V. Miakonkikh, D. S. Seregin, A. S. Vishnevskiy, K. A. Vorotilov, K. V. Rudenko, M. R. Baklanov, *J. Vac. Sci. Technol. A* **2020**, *38*, 033005.
[49] M. R. Baklanov, J.-F. de Marneffe, D. Shamiryan, A. M. Urbanowicz, H. Shi, T. V. Rakhimova, H. Huang, P. S. Ho, *J. Appl. Phys.* **2013**, *113*, 041101.
[50] P. Marsik, A. M. Urbanowicz, P. Verdonck, D. De Roest, H. Sprey, M. R. Baklanov, *Thin Solid Films* **2011**, *519*, 3619.
[51] A. I. Zotovich, S. M. Zyryanov, D. V. Lopaev, A. A. Rezvanov, A. G. Attallah, M. O. Liedke, M. Butterling, M. A. Bogdanova, A. S. Vishnevskiy, D. S. Seregin, D. A. Vorotyntsev, A. P. Palov, E. Hirschmann, A. Wagner, S. Naumov, K. A. Vorotilov, T. V. Rakhimova, A. T. Rakhimov, M. R. Baklanov, *ACS Appl. Electron. Mat.* **2022**, *4*, 2760.
[52] Y. Li, I. Ciofi, L. Carbonell, N. Heylen, J. Van Aelst, M. R. Baklanov, G. Groeseneken, K. Maex, Z. Tőkei, *J. Appl. Phys.* **2008**, *104*, 034113.
[53] M. T. Nichols, H. Sinha, C. A. Wiltbank, G. A. Antonelli, Y. Nishi, J. L. Shohet, *Appl. Phys. Lett.* **2012**, *100*, 112905.
[54] J. Lee, D. B. Graves, *J. Phys. D: Appl. Phys.* **2010**, *43*, 425201.
[55] D. V. Lopaev, S. M. Zyryanov, A. I. Zotovich, T. V. Rakhimova, Y. A. Mankelevich, A. T. Rakhimov, M. R. Baklanov, *Plasma Processes Polym.* **2018**, *15*, 1700213.
[56] T. H. DiStefano, D. E. Eastman, *Solid State Commun.* **1971**, *9*, 2259.
[57] V. K. Adamchuk, V. V. Afanasev, *Phys. Status Solidi A* **1992**, *132*, 371.
[58] V. V. Afanas'ev, *Internal Photoemission Spectroscopy*, Elsevier, **2014**.
[59] V. V. Afanas'ev, J. M. M. de Nijs, P. Balk, A. Stesmans, *J. Appl. Phys.* **1995**, *78*, 6481.
[60] H. Sinha, J. L. Lauer, M. T. Nichols, G. A. Antonelli, Y. Nishi, J. L. Shohet, *Appl. Phys. Lett.* **2010**, *96*, 052901.
[61] V. V. Afanas'ev, J. M. M. de Nijs, P. Balk, *Appl. Phys. Lett.* **1995**, *66*, 1738.
[62] E. Cartier, J. H. Stathis, D. A. Buchanan, *Appl. Phys. Lett.* **1993**, *63*, 1510.
[63] J. H. Stathis, E. Cartier, *Phys. Rev. Lett.* **1994**, *72*, 2745.
[64] H. Sinha, H. Ren, M. T. Nichols, J. L. Lauer, M. Tomoyasu, N. M. Russell, G. Jiang, G. A. Antonelli, N. C. Fuller, S. U. Engelmann, Q. Lin, V. Ryan, Y. Nishi, J. L. Shohet, *J. Appl. Phys.* **2012**, *112*, 111101.
[65] J. M. Atkin, D. Song, T. M. Shaw, E. Cartier, R. B. Laibowitz, T. F. Heinz, *J. Appl. Phys.* **2008**, *103*, 094104.
[66] Y. Li, A. Leśniewska, O. Varela Pedreira, J. F. de Marneffe, I. Ciofi, P. Verdonck, M. R. Baklanov, J. Bömmels, I. De Wolf, Z. Tőkei, K. Croes, *J. Appl. Phys.* **2015**, *118*, 164101.
[67] O. V. Braginsky, A. S. Kovalev, D. V. Lopaev, E. M. Malykhin, Y. A. Mankelevich, O. V. Proshina, T. V. Rakhimova, A. T. Rakhimov, D. G. Voloshin, A. N. Vasilieva,

S. M. Zyryanov, E. A. Smirnov, M. R. Baklanov, *J. Appl. Phys.* **2011**, *109*, 043303.

[68] A. S. Vishnevskiy, S. Naumov, D. S. Seregin, Y.-H. Wu, W.-T. Chuang, M. Rasadujjaman, J. Zhang, J. Leu, K. A. Vorotilov, M. R. Baklanov, *Materials* **2020**, *13*, 4484.

[69] J.-F. de Marneffe, L. Zhang, M. Heyne, M. Lukaszewicz, S. B. Porter, F. Vajda, V. Rutigliani, Z. el Otell, M. Krishtab, A. Goodyear, M. Cooke, P. Verdonck, M. R. Baklanov, *J. Appl. Phys.* **2015**, *118*, 133302.

[70] J. P. Perdew, K. Burke, M. Ernzerhof, *Phys. Rev. Lett.* **1996**, *77*, 3865.

[71] J. P. Perdew, K. Burke, M. Ernzerhof, *Phys. Rev. Lett.* **1997**, *78*, 1396.

[72] C. Adamo, V. Barone, *J. Chem. Phys.* **1999**, *110*, 6158.

[73] S. Grimme, J. Antony, S. Ehrlich, H. Krieg, *J. Chem. Phys.* **2010**, *132*, 154104.

[74] Jaguar. Version 9.6 Schrodinger Inc., New York, NY **2017**.

[75] R. Bauernschmitt, R. Ahlrichs, *Chem. Phys. Lett.* **1996**, *256*, 454.

[76] S. Yasuhara, J. Chung, K. Tajima, H. Yano, S. Kadomura, M. Yoshimaru, N. Matsunaga, S. Samukawa, *J. Phys. D: Appl. Phys.* **2009**, *42*, 235201.

How to cite this article: A. O. Serov, A. N. Ryabinkin, A. S. Vishnevskiy, S. Naumov, A. F. Pal, T. V. Rakhimova, D. S. Seregin, K. A. Vorotilov, M. R. Baklanov, *Plasma Processes Polym.* **2023**;20:e2200169. https://doi.org/10.1002/ppap.202200169